J. Fluid Mech. (1975), *vol.* 72, *part* 4, *pp.* 625–647
Printed in Great Britain

Initial flow field over an impulsively started circular cylinder

By M. BAR-LEV AND H. T. YANG
Department of Aerospace Engineering, University of Southern California, Los Angeles

(Received 28 April 1975)

The initial flow field of an incompressible, viscous fluid around a circular cylinder, set impulsively to move normal to its axis, is studied in detail. The nonlinear vorticity equation is solved by the method of matched asymptotic expansions. Analytic solutions for the stream function in terms of exponential and error functions for the inner flow field, and of circular functions for the outer, are obtained to the third order, from which a uniformly valid composite solution is found. Also presented are the vorticity, pressure, separation point and drag. These quantities agree with the numerical computations of Collins & Dennis. Extended solutions developed by Padé approximants indicate that higher tha n third-order approximations will yield only minor improvements.

1. Introduction

The analytic solution of the full Navier–Stokes equations for the flow field over an impulsively started circular cylinder is at present beyond our capabilities. In order to analyse the flow, one must resort to an iterative procedure. The method of matched asymptotic expansions was developed for a systematic treatment of such iteration.

Previous theoretical investigations of the initial flow over an impulsively started circular cylinder at finite Reynolds numbers consist notably of the work of Wang (1967) and of Collins & Dennis (1973*a*, *b*). Wang applied the method of inner and outer expansions. He formulated the problem in the spirit of boundary-layer theory, by solving the two momentum equations in polar co-ordinates. Assuming the solution to proceed in power series of the normalized time, he derived the first two approximations, within which the pressure is constant across the boundary. In the third approximation to be obtained, the pressure begins to vary across the viscous layer. Collins & Dennis (1973*a*) presented a somewhat different approach. They formulated the problem in the boundary-layer variables, and derived solutions for only the inner region. These were not matched with any outer solution, but adjusted to match the uniform flow far from the cylinder. They were expanded in powers of normalized time and boundary-layer variables. The first approximations were derived analytically, the succeeding were computed numerically to seventh order. Collins & Dennis (1973*b*) also numerically integrated the time-dependent Navier–Stokes equations for flow past an impulsively started circular cylinder. Their numerical

solution is satisfactory initially, in agreement with their earlier boundary-layer results (1973*a*). It is also valid at later times, when separation has begun and the viscous layer thickens, but before the wake becomes asymmetric.

In the present work, the formulation consists of only one governing nonlinear equation, that of the vorticity. The troublesome pressure field, which is unknown *a priori*, is thus eliminated. As a consequence, the resulting vorticity equation is one order higher than the momentum equations. However, an integration with the matching condition between inner and outer flows will reduce the order by one. The inner flow is governed to all orders by a linear partial differential equation, whose solution is related to the parabolic cylinder function. The outer flow is shown to be irrotational to the third order, governed by Laplace's equation. This makes the solution of the outer flow field particularly simple: mere inspection of the matching condition. The gauge functions in the asymptotic expansion are found by iteration, rather than assumed *a priori*. Inner and outer solutions to third order, and the resulting composite solutions, are obtained. The flow pattern is depicted, from which separation and eddy formation behind the cylinder are discernible. The vorticity and the strength of the vorticity source on the cylinder surface are calculated and plotted. Also presented are the progression of the separation point, the pressure distribution on the cylinder and the time history of drag. Padé approximants are used in an attempt to improve the results obtained. This seems to indicate that higher than third-order approximations add only minor corrections.

2. Matched asymptotic expansions

The governing vorticity equation for time-dependent, incompressible, viscous flow, Rosenhead (1963, p. 121), in non-dimensional form is

$$\frac{\partial \boldsymbol{\omega}}{\partial t} - \epsilon \nabla \times (\mathbf{V} \times \boldsymbol{\omega}) = \epsilon^2 \alpha \nabla^2 \boldsymbol{\omega}, \tag{1}$$

where

$$\epsilon = (U_0 T_0)/l_0 \qquad \alpha = (\epsilon Re)^{-1}. \tag{2}$$

In (2), l_0, T_0 and U_0 are respectively the reference length, time and velocity, $Re = (U_0 l_0)/\nu_0$ the Reynolds number. Hence, $Re = \frac{1}{2} R_d$, $R_d = (2U_0 r_0)/\nu_0$, the Reynolds number based on diameter. In our work, l_0 is the radius r_0 of the cylinder. For the initial phase of the flow, ϵ is a small quantity. For moderately large Reynolds number, α is finite. Consequently, we may expand the solution to (1) in only one parameter, ϵ. The original time variable may be recovered by the simple transformations

$$\epsilon t = \frac{U_0 t^*}{l_0} = T, \quad \epsilon(\alpha t)^{\frac{1}{2}} = (T/Re)^{\frac{1}{2}}. \tag{3}$$

Here t^* is the dimensional time, and T is a new non-dimensional time.

In polar co-ordinates, define a stream function ψ such that

$$u_r = -\frac{1}{r}\frac{\partial \psi}{\partial \theta}, \quad u_\theta = \frac{\partial \psi}{\partial r}. \tag{4}$$

The vorticity equation (1) then becomes

$$\left[\frac{\partial}{\partial t}+\epsilon\frac{1}{r}\left(\frac{\partial\psi}{\partial r}\frac{\partial}{\partial\theta}-\frac{\partial\psi}{\partial\theta}\frac{\partial}{\partial r}\right)-\epsilon^2\alpha\nabla^2\right]\nabla^2\psi=0, \tag{5}$$

in which

$$\nabla^2=\frac{\partial^2}{\partial r^2}+\frac{1}{r}\frac{\partial}{\partial r}+\frac{1}{r^2}\frac{\partial^2}{\partial\theta^2}.$$

It may be seen that, if the outer stream-function expansion consists of powers ϵ,

$$\psi^0=\psi_1^0+\sum_{n=2}\epsilon^{n-1}\psi_n^0, \tag{6}$$

then (5) with the initial condition of irrotationality gives

$$\nabla^2\psi_n^0=0, \quad n=2,3,\ldots. \tag{7}$$

In other words, the outer flow is irrotational to all orders of ϵ. To be more general than (6), the outer expansion is assumed to be of the form

$$\psi^0=\psi_1^0+\sum_{n=2}\delta_n(\epsilon)\,\psi_n^0. \tag{8}$$

In later matching procedures, the gauge functions $\delta_n(\epsilon)$ will be found to be as in (24) and (32):

$$\delta_n(\epsilon)=\epsilon^{n-1}, \quad n=2,3. \tag{9}$$

Therefore, to third order at least, the expansion (6) is valid and the outer flow remains irrotational, being governed by the Laplace equation (7). The leading term in the outer stream-function expansion is that of a potential uniform flow over a circular cylinder of unit radius:

$$\psi_1^0=(r-r^{-1})\sin\theta. \tag{10}$$

Since ψ_1^0 satisfies the uniform flow boundary condition at infinity, we require

$$\psi_n^0=0 \quad \text{as} \quad r\to\infty, \quad n=2,3,\ldots. \tag{11}$$

The solution to (7) satisfying condition (11) is

$$\psi_n^0=\sum_{k=1}r^{-k}[A_k(t)\sin k\theta+B_k(t)\cos k\theta], \quad n=2,3,\ldots. \tag{12}$$

The coefficients $A_k(t)$ and $B_k(t)$ will be determined by matching with the inner solution. The simple form of (12) will facilitate the solution for the outer flow field.

In the present singular perturbation problem, the region of non-uniformity near the cylinder should be stretched to unity order. Let the thickness of this region be $\Delta_1(\epsilon)$, which vanishes as ϵ vanishes. The proper stretching of the radial co-ordinate is then

$$R=(r-1)/\Delta_1(\epsilon). \tag{13}$$

In order to magnify the inner-flow stream function $\overline{\psi}^i$, which is a function of the stretched inner variable R, we set

$$\overline{\psi}^i(R,\theta,t)=\psi^i(r,\theta,t)/\delta(\epsilon). \tag{14}$$

By requiring that the tangential velocities inside and outside the inner region should be of the same order, we get, from (4), (13) and (14),

$$\delta(\epsilon) = \Delta_1(\epsilon). \tag{15}$$

The inner expansion of the stream function is assumed to be of the form

$$\psi^i(r, \theta, t; \epsilon) = \sum_{m=1} \Delta_m(\epsilon)\, \overline{\psi}^i_m(R, \theta, t), \tag{16}$$

in which $\Delta_m(\epsilon)$ are the gauge functions to be determined in (27) and (36).

3. First-order solution

Substituting the inner expansion (16) into the vorticity equation (5) and letting ϵ vanish, we get

$$\overline{\psi}^i_{1RRt} - \lim_{\epsilon \to 0} \left[\frac{\epsilon^2 \alpha}{\Delta_1^2(\epsilon)} \right] \overline{\psi}^i_{1RRRR} = 0.$$

Setting $\Delta_1(\epsilon) = \epsilon$, we get the linear equation governing the first-order inner expansion:

$$\overline{\psi}^i_{1RRt} - \alpha \overline{\psi}^i_{1RRRR} = 0. \tag{17}$$

Integration of (17) with respect to R yields

$$\overline{\psi}^i_{1Rt} - \alpha \overline{\psi}^i_{1RRR} = f(\theta, t). \tag{18}$$

The no-slip boundary conditions on the cylinder are, from (4),

$$\overline{\psi}^i_1(0, \theta, t) = 0, \quad \overline{\psi}^i_{1R}(0, \theta, t) = 0. \tag{19}$$

The matching condition is that the tangential velocity at the edge of the inner region $R \to \infty$ approaches that in the outer region as $r \to 1$. Employing the asymptotic principle (Van Dyke 1975, p. 90), we obtain

$$\overline{\psi}^i_{1R}(\infty, \theta, t) = \psi^0_{1r}(1, \theta, t), \tag{20}$$

where ψ^0_1 is given by (10). Applying matching condition (20) to (18) gives

$$f(\theta, t) = \psi^0_{1rt}(1, \theta, t) - \alpha \epsilon^2 \psi^0_{1rrr}(1, \theta, t) = 0, \tag{21}$$

by virtue of (10). The governing equation (18) is now identical to that for the impulsively started plate, the Rayleigh problem, except that the local first-order outer velocity on the cylinder should be used instead of the constant impulse velocity. The solution to (18) with (21) subject to the conditions (19) and (20) is

$$\overline{\psi}^i_{1R} = 2 \operatorname{erf} \eta \sin \theta, \quad \overline{\psi}^i_1 = \int_0^R \overline{\psi}^i_{1R}\, dR = 4(\alpha t)^{\frac{1}{2}} [\eta \operatorname{erf} \eta - \pi^{-\frac{1}{2}}(1 - \exp(-\eta^2))] \sin \theta, \tag{22}$$

where

$$\eta = R/[2(\alpha t)^{\frac{1}{2}}]. \tag{23}$$

We note that, on the cylinder surface, the normal derivative of the tangential velocity from (22) is always positive for $0 < \theta < \pi$. Therefore, the first-order expansion does not predict any flow separation. Equations (10) and (22) are the first-order solutions.

4. Second-order solution

Applying again the asymptotic matching principle (Van Dyke 1975, p. 90), with $m = 1$ in (16) and $n = 2$ in (8), we obtain

$$\delta_2(\epsilon) = \epsilon, \quad \psi_2^0(1,\theta,t) = -4\pi^{-\frac{1}{2}}(\alpha t)^{\frac{1}{2}}\sin\theta. \tag{24),(25}$$

Comparison of (12) with (25) yields the second-order outer solution

$$\psi_2^0(r,\theta,t) = -4\pi^{-\frac{1}{2}}(\alpha t)^{\frac{1}{2}} r^{-1}\sin\theta. \tag{26}$$

The contribution of (26) to the outer stream function is, through (3),

$$\epsilon\psi_2^0 = -4\pi^{-\frac{1}{2}}(T/Re)^{\frac{1}{2}} r^{-1}\sin\theta.$$

The effect is equivalent to that of a doublet, whose strength grows with the square root of time. The displacement is symmetric fore and aft of the circular cylinder, owing to the symmetry of the first-order inner solution (22).

The second-order inner solution may be found by setting $m = 2$ in (16) and $n = 2$ in (8) in the matching, with ψ_2^0 given by (26). We obtain

$$\Delta_2(\epsilon) = \epsilon^2, \quad \overline{\psi}_{2R}^i(\infty,\theta,t) = -2(R - 2\pi^{-\frac{1}{2}}(\alpha t)^{\frac{1}{2}})\sin\theta. \tag{27}$$

Substitution of (16) into (1) yields the second-order inner flow equation

$$\overline{\psi}_{2Rt}^i - \alpha\overline{\psi}_{2RRR}^i = 4\{1-(\operatorname{erf}\eta)^2 + 2\pi^{-\frac{1}{2}}\exp(-\eta^2)[\eta - \operatorname{erfc}\eta - \pi^{-\frac{1}{2}}(1-\exp(-\eta^2))]\} \times \sin\theta\cos\theta + 2\pi^{-\frac{1}{2}}(\alpha/t)^{\frac{1}{2}}(1+\exp(-\eta^2))\sin\theta. \tag{28}$$

The no-slip boundary conditions are

$$\overline{\psi}_{2R}^i(0,\theta,t) = 0, \quad \overline{\psi}_2^i(0,\theta,t) = 0. \tag{29}$$

The solution to (28), satisfying conditions (27) and (29), is

$$\begin{aligned}
\overline{\psi}_{2R}^i = {} & 2(\alpha t)^{\frac{1}{2}}\left[\frac{2}{\pi^{\frac{1}{2}}}(1-\exp(-\eta^2)) - 2\eta + 3\eta\operatorname{erfc}\eta\right]\sin\theta \\
& + 4t\left\{(\eta^2-\tfrac{1}{2})\operatorname{erfc}^2\eta - \frac{3}{\pi^{\frac{1}{2}}}\eta\exp(-\eta^2)\operatorname{erfc}\eta + \left[\left(\frac{1}{2}-\frac{2}{3\pi}\right) - \left(3+\frac{4}{3\pi}\right)\eta^2\right]\operatorname{erfc}\eta \right. \\
& \left. + \frac{4}{\pi^{\frac{1}{2}}}\left(1+\frac{1}{3\pi}\right)\eta\exp(-\eta^2) - \frac{4}{3\pi}\exp(-\eta^2) + \frac{2}{\pi}\exp(-2\eta^2)\right\}\sin\theta\cos\theta,
\end{aligned} \tag{30}$$

$$\begin{aligned}
\overline{\psi}_2^i = {} & \frac{4}{\pi^{\frac{1}{2}}}\alpha t\left[-\eta^2 + 2\eta - \frac{\pi^{\frac{1}{2}}}{4}(1-\operatorname{erfc}\eta) + \frac{3\pi^{\frac{1}{2}}}{2}\eta^2\operatorname{erfc}\eta - \tfrac{3}{2}\eta\exp(-\eta^2)\right]\sin\theta \\
& + 8t(\alpha t)^{\frac{1}{2}}\left[\frac{11}{6\pi^{\frac{1}{2}}}\exp(-\eta^2)\operatorname{erfc}\eta - \frac{8}{3(2\pi)^{\frac{1}{2}}}\operatorname{erfc}\sqrt{2}\,\eta\right. \\
& + \tfrac{1}{3}\eta^3\operatorname{erfc}^2\eta - \frac{2}{3\pi^{\frac{1}{2}}}\eta^2\exp(-\eta^2)\operatorname{erfc}\eta + \frac{1}{3\pi}\eta\exp(-2\eta^2) - \tfrac{1}{2}\eta\operatorname{erfc}^2\eta \\
& + \left(\frac{4}{9\pi}-\frac{3}{2}\right)\pi^{-\frac{1}{2}}\exp(-\eta^2) - \left(1+\frac{4}{9\pi}\right)\eta^3\operatorname{erfc}\eta + \left(1+\frac{4}{9\pi}\right)\pi^{-\frac{1}{2}}\eta^2\exp(-\eta^2) \\
& \left. + \frac{2}{3\pi^{\frac{1}{2}}}\operatorname{erfc}\eta + \left(\frac{1}{2}-\frac{2}{3\pi}\right)\eta\operatorname{erfc}\eta + \left(\frac{8}{3\sqrt{2}}-\frac{4}{9\pi}-1\right)\pi^{-\frac{1}{2}}\right]\sin\theta\cos\theta.
\end{aligned} \tag{31}$$

We have recovered Blasius's solution (Schlichting 1968, p. 400; Rosenhead 1963, p. 372) and Wang's correction for finite Reynolds numbers (Wang 1967). The first term in (30) is symmetric about the 90° radius, but the second is not; in fact, it is negative over the rear of the cylinder. (See Schlichting 1968, figure 15.1.) This part of the solution will cause thickening of the boundary layer at the rear of the cylinder and, eventually, separation and back flow. The second-order solution consists of (26) and (31).

5. Third-order solution

Using the asymptotic matching principle with $m = 2$ in (16), $n = 3$ in (8) and the second-order solution (26) and (31), we get the third-order gauge function and the matching condition

$$\delta_3(\epsilon) = \epsilon^2, \tag{32}$$

$$\psi_3^0(1,\theta,t) = -\alpha t \sin\theta + 8t(\alpha t)^{\frac{1}{2}}\pi^{-\frac{1}{2}}\left(\frac{8}{3\sqrt{2}} - \frac{4}{9\pi} - 1\right)\sin\theta\cos\theta. \tag{33}$$

Comparison of (12) and (33) determines

$$\psi_3^0 = -\alpha t r^{-1}\sin\theta + 8t(\alpha t)^{\frac{1}{2}}\pi^{-\frac{1}{2}}\left(\frac{8}{3\sqrt{2}} - \frac{4}{9\pi} - 1\right) r^{-2}\sin\theta\cos\theta. \tag{34}$$

The contribution of the third-order outer expansion to the outer expansion is, through (3),

$$\epsilon^2\psi_3^0 = -(T/Re)\, r^{-1}\sin\theta + 8T(T/Re)^{\frac{1}{2}}\pi^{-\frac{1}{2}}\left(\frac{8}{3\sqrt{2}} - \frac{4}{9\pi} - 1\right) r^{-2}\sin\theta\cos\theta. \tag{35}$$

The first part is equivalent to a doublet with strength symmetrical around the top of the cylinder, the second is a quadrupole, the strength of which is no longer symmetrical around the top. This will cause displacement that is more pronounced at the rear of the cylinder.

A correction is needed in the inner flow, to take care of the modification of the velocity at its boundary owing to the third-order outer flow. Matching the tangential velocities with $m = 3$ in (16) and $n = 3$ in (8) gives

$$\Delta_3(\epsilon) = \epsilon^3,$$

$$\overline{\psi}_{3R}^i(\alpha,\theta,t) = 3R^2\sin\theta - \frac{8}{\pi^{\frac{1}{2}}}(\alpha t)^{\frac{1}{2}} R\sin\theta + \alpha t\sin\theta - \frac{16}{\pi^{\frac{1}{2}}} t(\alpha t)^{\frac{1}{2}}\left(\frac{8}{3\sqrt{2}} - \frac{4}{9\pi} - 1\right)\sin\theta\cos\theta. \tag{36}$$

Substituting the inner expansion (16) into the vorticity equation (11), eliminating the parts that correspond to (17) and (28), and letting ϵ vanish, we get the equation for the third-order inner flow:

$$\begin{aligned}\overline{\psi}_{3RRt}^i - \alpha\overline{\psi}_{3RRRR}^i = &-\overline{\psi}_{2Rt}^i + R\overline{\psi}_{1Rt}^i - \overline{\psi}_{10\theta t}^i - \overline{\psi}_{1R}^i\overline{\psi}_{2RR\theta}^i - \overline{\psi}_{2R}^i\overline{\psi}_{1RR\theta}^i + \overline{\psi}_{1\theta}^i\overline{\psi}_{2RRR}^i \\ &- \overline{\psi}_{1R}^i\overline{\psi}_{1R\theta}^i + R\overline{\psi}_{1R}^i\overline{\psi}_{1RR\theta}^i + \overline{\psi}_{1\theta}^i\overline{\psi}_{1RR}^i - R\overline{\psi}_{1\theta}^i\overline{\psi}_{1RRR}^i \\ &+ \overline{\psi}_{2\theta}^i\overline{\psi}_{1RRR}^i + \alpha[2\overline{\psi}_{2RRR}^i - 2R\overline{\psi}_{1RRR}^i + 2\overline{\psi}_{1RR\theta\theta}^i - \overline{\psi}_{1RR}^i].\end{aligned} \tag{37}$$

The boundary conditions are the matching conditions (36) and the no-slip conditions on the boundary,

$$\overline{\psi}^i_3(0,\theta,t) = 0, \quad \overline{\psi}^i_{3R}(0,\theta,t) = 0. \tag{38), (39}$$

We integrate (37) and use the matching condition (36) to evaluate the constant of integration. The solution is

$$\overline{\psi}^i_{3R} = \alpha t \sin\theta f_1(\eta) + 8t(\alpha t)^{\frac{1}{2}} \sin\theta\cos\theta g(\eta) + 8t^2[\sin\theta\cos^2\theta f_3(\eta) - \sin^3\theta F_3(\eta)], \tag{40}$$

where

$$\left.\begin{aligned} f_1(\eta) &= 1 - \frac{16}{\pi^{\frac{1}{2}}}\eta + 12\eta^2 - \operatorname{erfc}\eta - 32\eta^2\operatorname{erfc}\eta + \frac{29}{\pi^{\frac{1}{2}}}\eta\exp(-\eta^2), \\ g(\eta) &= \tfrac{1}{2}\eta\operatorname{erfc}^2\eta + \tfrac{3}{4}\eta\operatorname{erfc}^2\eta + \left(\frac{51}{8} + \frac{14}{9\pi} - \frac{7\sqrt{2}}{2}\right)\eta^3\operatorname{erfc}\eta \\ &\quad + \left(\frac{89}{16} + \frac{5}{3\pi} - \frac{21\sqrt{2}}{4}\right)\eta\operatorname{erfc}\eta + \frac{2}{3\pi^{\frac{1}{2}}}\operatorname{erfc}\eta + \frac{1}{4\pi^{\frac{1}{2}}}\exp(-\eta^2)\operatorname{erfc}\eta \\ &\quad + \pi^{-\frac{1}{2}}\eta^2\exp(-\eta^2)\operatorname{erfc}\eta + \pi^{-\frac{1}{2}}\left(\frac{7\sqrt{2}}{2} - \frac{35}{12} - \frac{8}{9\pi}\right)\exp(-\eta^2) + \frac{28}{15\pi}\eta\exp(-\eta^2) \\ &\quad - \pi^{-\frac{1}{2}}\left(\frac{181}{24} + \frac{14}{9\pi} - \frac{7\sqrt{2}}{2}\right)\eta^2\exp(-\eta^2) - \tfrac{5}{6}(2/\pi)^{\frac{1}{2}}\operatorname{erfc}\sqrt{2}\,\eta \\ &\quad - \frac{7}{6\pi}\eta\exp(-2\eta^2) - \frac{2}{\pi^{\frac{1}{2}}}\left(\frac{4\sqrt{2}}{3} - 1 - \frac{4}{9\pi}\right), \end{aligned}\right\} \tag{40a}$$

$$\begin{aligned} F_3(\eta) &= \tfrac{1}{12}(4\eta^4+3)\operatorname{erf}^3\eta \\ &\quad + \left[\frac{1}{8}\left(1+\frac{4}{3\pi}\right)(4\eta^4+4\eta^2-1) + \frac{1}{12\pi^{\frac{1}{2}}}(14\eta^3-9\eta)\exp(-\eta^2)\right]\operatorname{erf}^2\eta \\ &\quad + \left[2\left(1+\frac{2}{3\pi}\right)\eta^2 + \tfrac{1}{2} + \frac{2}{3\pi} + \frac{1}{12\pi^{\frac{1}{2}}}\left(1+\frac{4}{3\pi}\right)(14\eta^3+15\eta)\exp(-\eta^2)\right. \\ &\quad \left. + \frac{1}{3\pi}(4\eta^2-5)\exp(-2\eta^2)\right]\operatorname{erf}\eta \\ &\quad + \frac{1}{30\pi^{\frac{1}{2}}}\left[-10\left(1+\frac{2}{3\pi}\right)\eta^3 - 35 - \frac{10}{\pi} - \frac{8}{\pi^{\frac{1}{2}}}\left(1+\frac{4}{3\pi}\right)\right]\exp(-\eta^2) \\ &\quad + \frac{2}{3\pi}\left(1+\frac{4}{3\pi}\right)(\eta^2+1)\exp(-2\eta^2) - \frac{1}{40\pi\,\pi^{\frac{1}{2}}}(18\eta^3+31\eta)\exp(-3\eta^2) \\ &\quad + \frac{16\sqrt{2}}{15\pi}\exp(-\eta^2)\operatorname{erf}\sqrt{2}\,\eta - \frac{9\sqrt{3}}{80\pi}(4\eta^4+12\eta^2+3)\operatorname{erf}\sqrt{3}\,\eta \\ &\quad - \left(\frac{8}{45\pi^2} + \frac{2}{15\pi}\right)(4\eta^4+12\eta^2+3) - \left(\frac{5}{24} + \frac{1}{30\pi} - \frac{8}{45\pi^2} - \frac{\sqrt{3}}{5\pi^2}\right) \\ &\quad \times [(4\eta^4+12\eta^2+3)\operatorname{erf}\eta + \pi^{-\frac{1}{2}}(4\eta^3+10\eta\exp(-\eta^2)], \end{aligned} \tag{40b}$$

$$
\begin{aligned}
f_3(\eta) = F_3(\eta) &- \tfrac{1}{3}(2\eta^4+3\eta^2)\operatorname{erf}^3\eta \\
&- \left[\frac{1}{12\pi}\left(1+\frac{4}{3\pi}\right)(4\eta^3+3)+\frac{4}{3\pi}\eta+\frac{5}{2\pi^{\frac{1}{2}}}(\eta^3+\eta)\exp(-\eta^2)\right]\operatorname{erf}^2\eta \\
&- \left\{\frac{1}{6}\left[\left(12+\frac{8}{\pi}\right)\eta^2-\frac{8}{\pi^{\frac{1}{2}}}\left(1+\frac{4}{3\pi}\right)\eta-3\right]+\frac{2}{3\pi}\left[\pi^{\frac{1}{2}}\left(1+\frac{4}{3\pi}\right)(\eta^3-\eta)-2\eta+1\right]\right. \\
&\left.+\frac{3}{\pi}(\eta^2+1)\exp(-2\eta^2)\right\}\operatorname{erf}\eta \\
&+ \frac{8}{3\pi^{\frac{1}{2}}}\left(1+\frac{2}{3\pi}\right)\eta-\frac{4}{3\pi^{\frac{1}{2}}}\left[\left(2+\frac{2}{\pi}\right)\eta+\pi^{-\frac{1}{2}}\left(1+\frac{4}{3\pi}\right)\right]\exp(-\eta^2) \\
&- \frac{1}{3\pi\pi^{\frac{1}{2}}}\left[\pi^{\frac{1}{2}}\left(1+\frac{4}{3\pi}\right)(\eta^2-2)-4\eta\right]\exp(-2\eta^2) \\
&+ \frac{1}{24\pi\pi^{\frac{1}{2}}}(54\eta^3+125\eta)\exp(-3\eta^2)+\frac{9\sqrt{3}}{16\pi}(4\eta^4+12\eta^2+3)\operatorname{erf}\sqrt{3}\,\eta \\
&+ \left(\frac{8}{27\pi^2}+\frac{2}{9\pi}\right)(4\eta^4+12\eta^2+3) \\
&- \left(\frac{8}{27\pi^2}+\frac{1}{9\pi}+\frac{9\sqrt{3}}{16\pi}-\frac{1}{4}\right)\left[(4\eta^4+12\eta^2+3)\operatorname{erf}\eta+\frac{2}{\pi^{\frac{1}{2}}}(2\eta^3+5\eta)\exp(-\eta^2)\right].
\end{aligned}
\tag{40c}
$$

The third-order solution consists of (34) and (40).

6. Composite solution

Having an outer expansion valid in the outer region, and an inner expansion valid in the inner region, we can form a single composite solution which is uniformly valid throughout the whole flow field. We form the composite solution by summing the inner and outer expansions and subtracting out the common part. The common part is the matching quantity we derived in each of the matching procedures. Performing the composition to the third-order expansion, we get (see Van Dyke 1975, p. 94)

$$
\begin{aligned}
\psi_r = \sin\theta(1+r^{-2}-2\operatorname{erfc}\eta)&+\frac{2T^{\frac{1}{2}}}{Re^{\frac{1}{2}}}\sin\theta\left(\frac{2}{\pi^{\frac{1}{2}}r^2}-\frac{2}{\pi^{\frac{1}{2}}}\exp(-\eta^2)+3\eta\operatorname{erfc}\eta\right) \\
&+ 4T\sin\theta\cos\theta\left\{(\eta^2-\tfrac{1}{2})\operatorname{erfc}^2\eta-\frac{3}{\pi^{\frac{1}{2}}}\eta\exp(-\eta^2)\operatorname{erfc}\eta\right. \\
&+ \left[\left(\frac{1}{2}-\frac{2}{3\pi}\right)-\left(3+\frac{4}{3\pi}\right)\eta^2\right]\operatorname{erfc}\eta+\frac{4}{\pi^{\frac{1}{2}}}\left(1+\frac{1}{3\pi}\right)\eta\exp(-\eta^2) \\
&\left.-\frac{4}{3\pi}\exp(-\eta^2)+\frac{2}{\pi}\exp(-2\eta^2)\right\} \\
&+ \frac{T}{Re}\sin\theta\left(r^{-2}-\operatorname{erfc}\eta-32\eta^2\operatorname{erfc}\eta+\frac{29}{\pi^{\frac{1}{2}}}\eta\exp(-\eta^2)\right) \\
&+ 8\frac{TT^{\frac{1}{2}}}{Re^{\frac{1}{2}}}\sin\theta\cos\theta\left[-\frac{2}{\pi^{\frac{1}{2}}}\left(\frac{4\sqrt{2}}{3}-1-\frac{4}{9\pi}\right)\frac{1}{r^3}\right. \\
&\left.+\frac{2}{\pi^{\frac{1}{2}}}\left(\frac{4\sqrt{2}}{3}-1-\frac{4}{9\pi}\right)+g(\eta)\right] \\
&+ 8T^2[\sin\theta\cos^2\theta f_3(\eta)-\sin^3\theta F_3(\eta)],
\end{aligned}
\tag{41}
$$

$$\psi = \sin\theta\,(r-r^{-1}) + \frac{4T^{\frac{1}{2}}}{Re^{\frac{1}{2}}}\sin\theta\,\pi^{-\frac{1}{2}}\,(-r^{-1} - \pi^{\frac{1}{2}}\eta\,\mathrm{erfc}\,\eta + \exp(-\eta^2))$$
$$+ \frac{T}{Re}\sin\theta\left(-r^{-1} + \mathrm{erfc}\,\eta + 6\eta^2\,\mathrm{erfc}\,\eta - \frac{6}{\pi^{\frac{1}{2}}}\eta\exp(-\eta^2)\right)$$
$$+ 8\frac{TT^{\frac{1}{2}}}{Re}\sin\theta\cos\theta\left[\pi^{-\frac{1}{2}}\left(\frac{4\sqrt{2}}{3} - 1 - \frac{4}{9\pi}\right)r^{-1} + \frac{11}{6\pi^{\frac{1}{2}}}\exp(-\eta^2)\,\mathrm{erfc}\,\eta\right.$$
$$- \tfrac{4}{3}(2/\pi)^{\frac{1}{2}}\,\mathrm{erfc}\,\sqrt{2}\eta + \tfrac{1}{3}\eta^3\,\mathrm{erfc}^2\,\eta - \frac{2}{3\pi^{\frac{1}{2}}}\eta^2\exp(-\eta^2)\,\mathrm{erfc}\,\eta$$
$$+ \frac{1}{3\pi}\eta\exp(-2\eta^2) - \tfrac{1}{2}\eta\,\mathrm{erfc}^2\,\eta - \pi^{-\frac{1}{2}}\left(\frac{3}{2} - \frac{4}{9\pi}\right)\exp(-\eta^2)$$
$$\left. - \left(1 + \frac{4}{9\pi}\right)\eta^3\,\mathrm{erfc}\,\eta + \pi^{-\frac{1}{2}}\left(1 + \frac{4}{9\pi}\right)\eta^2\exp(-\eta^2) + \frac{2}{3\pi^{\frac{1}{2}}}\,\mathrm{erfc}\,\eta + \left(\frac{1}{2} - \frac{2}{3\pi}\right)\eta\,\mathrm{erfc}\,\eta\right]$$
$$+ 2\frac{TT^{\frac{1}{2}}}{ReRe^{\frac{1}{2}}}\sin\theta\left[-\eta\,\mathrm{erfc}\,\eta + \frac{15}{6\pi^{\frac{1}{2}}}(1 - \exp(-\eta^2))\right.$$
$$\left. + \tfrac{32}{3}\eta^2\,\mathrm{erfc}\,\eta + \frac{32}{3\pi^{\frac{1}{2}}}\eta^2\exp(-\eta^2)\right]$$
$$+ \frac{16T^2}{Re}\sin\theta\cos\theta\left[\tfrac{1}{24}\eta^4\,\mathrm{erfc}^2\,\eta + \tfrac{1}{4}\eta^3\,\mathrm{erfc}^2\,\eta + \tfrac{7}{32}(1 - \mathrm{erfc}^2\,\eta)\right.$$
$$- \frac{1}{12\pi^{\frac{1}{2}}}\eta^3\exp(-\eta^2)\,\mathrm{erfc}\,\eta - \frac{5}{8\pi^{\frac{1}{2}}}\eta\exp(-\eta^2)\,\mathrm{erfc}\,\eta - \frac{1}{2\pi^{\frac{1}{2}}}\eta^2\exp(-\eta^2)\,\mathrm{erfc}\,\eta$$
$$+ \pi^{-\frac{1}{2}}(1 - \exp(-\eta^2)\,\mathrm{erfc}\,\eta) + \frac{1}{4}\left(\frac{51}{8} + \frac{14}{9\pi} - \frac{7\sqrt{2}}{2}\right)\eta^4\,\mathrm{erfc}\,\eta - \frac{2}{3\pi^{\frac{1}{2}}}\eta\,\mathrm{erfc}\,\eta$$
$$+ \left(\frac{7\sqrt{2}}{2} - \frac{275}{128} - \frac{13}{24\pi}\right)\mathrm{erf}\,\eta - \tfrac{5}{6}(2/\pi)^{\frac{1}{2}}\eta\,\mathrm{erfc}\,\sqrt{2}\,\eta - \tfrac{5}{16}(2/\pi)^{\frac{1}{2}}\,\mathrm{erf}\,\sqrt{2}\eta$$
$$- \left(\frac{51}{8} + \frac{14}{9\pi} - \frac{7\sqrt{2}}{2}\right)\frac{1}{4\pi^{\frac{1}{2}}}\eta^3\exp(-\eta^2) + \frac{1}{24\pi}\eta^2\exp(-2\eta^2)$$
$$+ \left(\frac{265}{192} + \frac{7}{36\pi} - \frac{7\sqrt{2}}{10}\right)\pi^{-\frac{1}{2}}\eta\exp(-\eta^2)$$
$$+ \frac{4}{15\pi}(1 - \exp(-\eta^2)) + \frac{1}{4\pi}\eta\exp(-2\eta^2) - \frac{11}{8\pi}(1 - \exp(-2\eta^2))$$
$$\left. + \frac{16T^2T^{\frac{1}{2}}}{Re^{\frac{1}{2}}}\left[\sin\theta\cos^2\theta\int_0^\eta f_3(\eta)\,d\eta - \sin^3\theta\int_0^\eta F_3(\eta)\,d\eta\right]\right. . \tag{42}$$

Note that

$$\eta = (r-1)\,Re^{\frac{1}{2}}/2T^{\frac{1}{2}}.$$

7. Flow properties

The velocity profiles (41) and lines of constant stream function (42) for $Re = 500$ ($R_d = 1000$) and $T = 1{\cdot}0$ are plotted in figure 1. As we shall see in figure 7, separations started before $T = 0{\cdot}4$, and back flow occurs in the separated flow region.

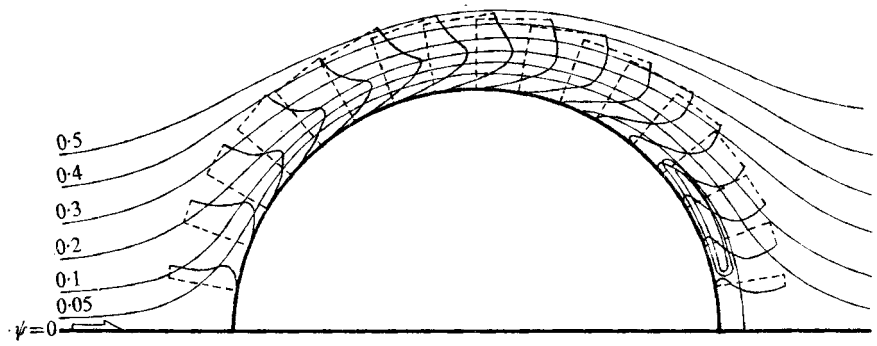

FIGURE 1. Velocity profiles and streamlines at $R_d = 2Re = 1000$, $T = 1$.

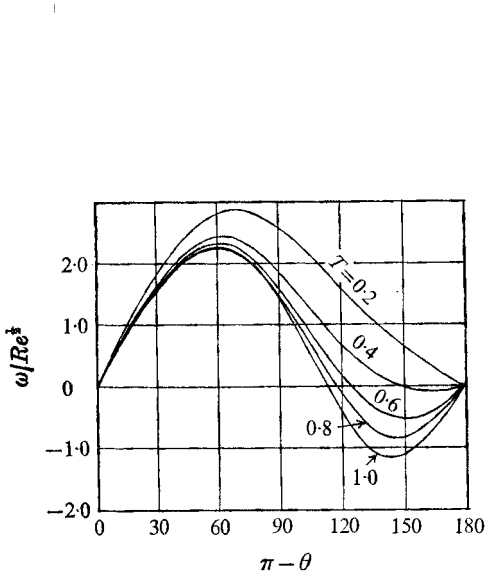

FIGURE 2

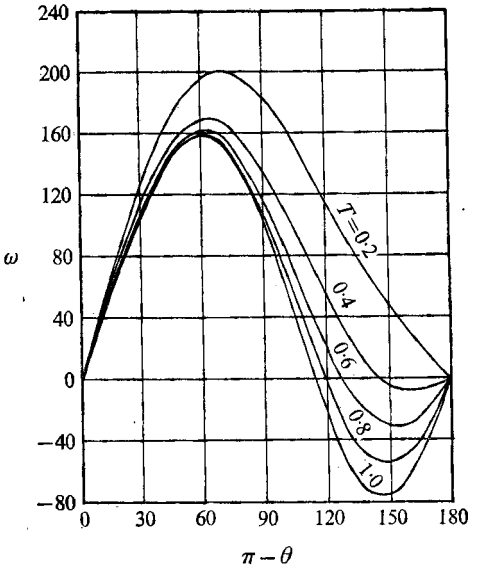

FIGURE 3

FIGURE 2. Vorticity distribution on the cylinder at $R_d = 2Re = \infty$.
FIGURE 3. Vorticity distribution on the cylinder at $R_d = 2Re = 10000$.

In the case of an impulsively started cylinder, the fluid is initially free of vorticity. As the cylinder moves through the fluid, vorticity is generated at the solid surface, shed and diffuses into the fluid. On the cylinder surface $r = r_0$, the vorticity is

$$\omega_{(r_0)} = \psi_{rr(r_0)} = \frac{2}{\pi^{\frac{1}{2}}}\frac{Re^{\frac{1}{2}}}{T^{\frac{1}{2}}}\sin\theta + \sin\theta + \frac{4}{\pi^{\frac{1}{2}}}\left(1+\frac{4}{3\pi}\right)Re^{\frac{1}{2}}T^{\frac{1}{2}}\sin\theta\cos\theta$$
$$+\frac{15}{2\pi^{\frac{1}{2}}}\frac{T^{\frac{1}{2}}}{Re^{\frac{1}{2}}}\sin\theta - 4\left(7\sqrt{2}-\frac{101}{16}-\frac{58}{15\pi}\right)T\sin\theta\cos\theta$$
$$-\frac{8}{\pi^{\frac{1}{2}}}Re^{\frac{1}{2}}T^{\frac{3}{2}}\left[\left(\frac{108\sqrt{3}-89}{30\pi}+\frac{128}{135\pi^2}-\frac{11}{12}\right)\sin\theta\cos^2\theta\right.$$
$$\left.+\left(\frac{64}{45\pi^2}+\frac{27\sqrt{3}-11}{30\pi}-\frac{7}{12}\right)\sin^3\theta\right]. \qquad (43)$$

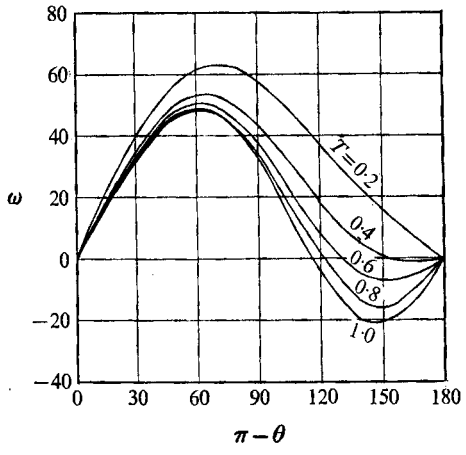

FIGURE 4. Vorticity distribution on the cylinder at $R_d = 2Re = 1000$.

θ	0	45	90	135	180
			$T = 0{\cdot}2$		
Collins & Dennis (1973*a*, figure 3)	0	1·74	1·80	0·73	0
Collins & Dennis (1973*b*, figure 13)	0	1·77	1·80	0·72	0
Present	0	1·749	1·788	0·733	0
			$T = 0{\cdot}4$		
Collins & Dennis (1973*a*, figure 3)	0	1·56	1·30	0·13	0
Collins & Dennis (1973*b*, figure 13)	0	1·57	1·30	0·11	0
Present	0	1·565	1·310	0·127	0
			$T = 1{\cdot}0$		
Belcher *et al.* (1972, figure 1)	0	1·52	1·0	−0·79	0
Collins & Dennis (1973*a*, figure 3)	0	1·50	1·0	−0·78	0
Collins & Dennis (1973*b*, figure 13)	0	1·50	1·0	−0·78	0
Present	0	1·520	0·989	−0·767	0

TABLE 1. Comparison of the vorticity distribution $\omega R_d^{-\frac{1}{2}} \equiv \omega(2Re)^{-\frac{1}{2}}$ on the cylinder at $Re = \infty$

θ	0	45	90	135	180
			$T = 0{\cdot}2$		
Collins & Dennis (1973*b*, figure 11)	0	26·0	58·0	55·0	0
Present	0	25·02	58·04	55·28	0
			$T = 1{\cdot}0$		
Collins & Dennis (1973*b*, figure 11)	0	−10·9	30·00	45·0	0
Present	0	−18·26	32·45	44·20	0

TABLE 2. Comparison of the vorticity distribution on the cylinder at $R_d = 2Re = 1000$

The vorticity distribution on the cylinder is plotted in figures 2–4 for various Reynolds numbers. Table 1 compares the vorticity distribution

$$\omega(\theta)/R_d^{\frac{1}{2}} \equiv \omega(\theta)/Re^{\frac{1}{2}}$$

on the cylinder at $Re = \infty$ of Collins & Dennis (1973*a*, *b*) with the present analytic results, at $T = 0{\cdot}2$, $0{\cdot}4$ and $1{\cdot}0$. For the case $T = 1{\cdot}0$, the numerical computation of Belcher, Burggraf, Cooke, Robins & Stewartson (1972) is also included. The agreement is seen to be very good. Table 2 compares the vorticity distributions $\omega(\theta)$ also at $R_d = 2Re = 1000$ for $T = 0{\cdot}2$ and $1{\cdot}0$. It is seen that agreement is again very good at small times. When $T = 1{\cdot}0$, where the present expansion is not expected to be valid, the agreement is less satisfactory, particularly in the rear separated flow region. A vortex sheet, represented by the singular first term, forms on the surface at the impulsive start $T \to 0$. Later, the vorticity diffuses out into the fluid. The gradient of vorticity at the rear stagnation point, which is negative initially, grows positive, indicating separation and back flow.

It is of interest to develop the vorticity gradient along the normal to the surface, which is the flow of vorticity per unit area per unit time out of the surface. This quantity, multiplied by $-\nu$, may be termed the strength of the local vorticity source $S = -\nu(\partial\omega/\partial r)_{r_0}$. Normalizing S as $\bar{S} = U_0^2 S/r_0$, we get

$$\begin{aligned}\bar{S} = Re^{-1}\Big\{&\frac{2}{\pi^{\frac{1}{2}}}\frac{Re^{\frac{1}{2}}}{T^{\frac{1}{2}}}\sin\theta + 4Re\sin\theta\cos\theta + \left(9-\frac{15}{\pi^{\frac{1}{2}}}\right)\sin\theta \\ &-4\left(\frac{303}{16}-21\sqrt{2}+\frac{26}{5\pi}-\frac{17}{\pi^{\frac{1}{2}}}-\frac{4}{\pi^{\frac{3}{2}}}+\frac{69\sqrt{2}}{2\pi^{\frac{1}{2}}}\right)Re^{\frac{1}{2}}T^{\frac{1}{2}}\sin\theta\cos\theta \\ &-\frac{15}{2\pi^{\frac{1}{2}}}\frac{T^{\frac{1}{2}}}{Re^{\frac{1}{2}}}\sin\theta - 4\left(7\sqrt{2}-\frac{101}{16}-\frac{58}{15\pi}\right)T\sin\theta\cos\theta \\ &+\frac{8}{\pi^{\frac{1}{2}}}Re^{\frac{1}{2}}T^{\frac{3}{2}}\left[\left(\frac{108\sqrt{3}-89}{30\pi}+\frac{128}{135\pi^2}-\frac{11}{12}\right)\sin\theta\cos^2\theta\right. \\ &\left.+\left(\frac{64}{45\pi^2}+\frac{27\sqrt{3}-11}{30\pi}-\frac{7}{12}\right)\sin^3\theta\right]\Big\}. \end{aligned} \tag{44}$$

The strength of the vorticity sources along the cylinder is plotted in figures 5 and 6. Note that the higher the Reynolds number or the less viscous the flow, the less is the decrease with time of the vorticity strength. For the initial time, the viscous-layer thickness is of order $(\nu t)^{\frac{1}{2}}$, thinner for less viscous flow; then the vorticity source on the surface must adjust the velocity jump over a thinner layer.

The separation point on the cylinder is the point at which the vorticity vanishes (which means that the streamlines close to the surface are no longer parallel to it) and the vorticity gradient along the cylinder is negative, indicating a normal flow away from the cylinder. To find the separation point, we set the vorticity on the cylinder (43) to zero. Differentiating with respect to the tangential co-ordinate θ, we see that the separation starts always at the rear stagnation point. The progression with time of the separation point is plotted in figure 7 for different Reynolds numbers. We observe that the separation angle tends

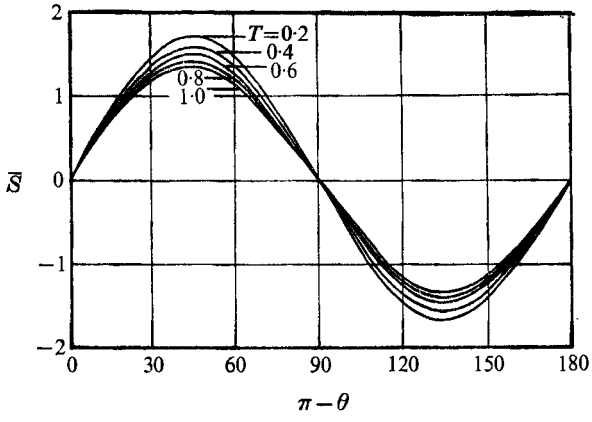

FIGURE 5. Strength of surface vorticity source at $R_d = 2Re = 2000$.

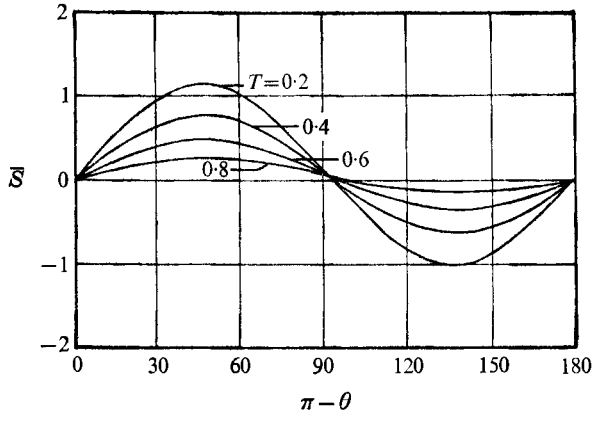

FIGURE 6. Strength of surface vorticity source at $R_d = 2Re = 200$.

asymptotically to some value which is, presumably, the steady separation angle. The lower the Reynolds number, the closer this angle to the rear stagnation point. The time of the initial separation at the rear stagnation point is plotted in figure 8. Also plotted for comparison are the curve of Wang (1967), which uses only the second-order expansion, and the two curves obtained numerically by Collins & Dennis (1973*a*, *b*). The third-order expansion curve is close to that predicted by Collins & Dennis, although somewhat lower. At $R_d = 2Re = 500$, the values of separation time found by Collins & Dennis are $T_s = 0{\cdot}396$ (1973*a*) and $T_s = 0{\cdot}394$ (1973*b*). See Collins & Dennis (1973*b*, table 3). Our analytic result is 0·365, which is in close agreement with the recent numerical result of 0·37 obtained by Panikker & Lavan (1975). For $Re \to \infty$, the second-order solution for the initial separation time is the same as that of Blasius, which was also obtained by Wang (1967), namely,

$$T = \left(2+\frac{8}{3\pi}\right)^{-1} = 0{\cdot}351.$$

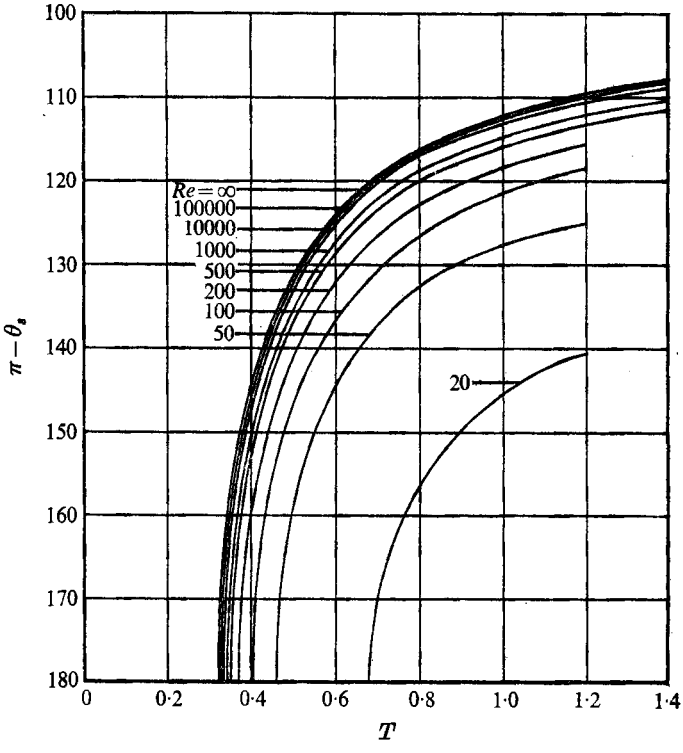

FIGURE 7. Progression of separation point.

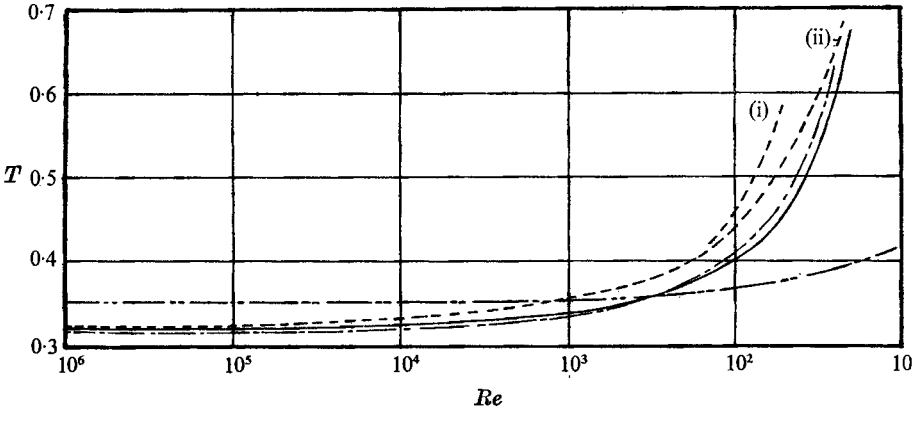

FIGURE 8. Time of initial separation. – – – –, (i), (ii), Collins & Dennis (1973*a*, *b*); – – – –, second order expansion Wang (1967);——, third order expansion; — · —, Padé approximant [2/2].

θ	180	166	146	138	124	110
			$Re = \infty$			
Collins & Dennis (1973*a*, figure 2)	0·322	0·331	0·39	0·43	0·589	0·90
Collins & Dennis (1973*b*, figure 6)	0·322	0·33	0·39	0·42	0·59	1·10
Sears & Telionis (1975, figure 10)†	0·35‡	0·36	0·40	0·45	0·60	1·11
Present	0·322	0·330	0·389	0·438	0·602	1·089

† Trajectory of zero wall shear. ‡ Telionis & Tsahalis (1974, p. 1496).

TABLE 3. Comparison of progression of separation point at $Re = \infty$

The third-order solution is the same as that of Goldstein and Rosenhead, which was obtained by Collins & Dennis (1973*a*, (75)), namely,

$$T = \left[-\left(1+\frac{4}{3\pi}\right)+\left(\frac{752}{135\pi^2}+\frac{216\sqrt{3}-138}{15\pi}-\frac{8}{3}\right)^{\frac{1}{2}}\right]\left(\frac{512}{135\pi^2}-\frac{11}{3}+\frac{216\sqrt{3}-178}{15\pi}\right)^{-1}$$

$$= 0{\cdot}3195.$$

The first term of Collins & Dennis (1973*a* (75)), or the denominator above multiplied by T^2, is the additional term $\omega_{02}(x,\theta)$ of Collins & Dennis (1973*a*). Thus, the inadequacy of Wang's results is removed by the present third-order expansion. In fact, it is the senior author's perception of this improvement that motivated the present study. Incidentally, the curve of Wang in Collins & Dennis (1973*a*, figure 1) should be displaced as in our figure 8. By the Padé approximant, the improved initial separation time for $Re \to \infty$ is a little shorter as shown in figure 8, contrary to the results of Collins & Dennis. The definition of the separation point in unsteady boundary-layer flow is currently much under discussion. (See Riley 1975.) Since the present analysis is based on the full Navier–Stokes equations, the definition proposed by Sears & Telionis (1975) in unsteady boundary-layer equation solutions involving Goldstein singularities does not apply here. The definition given at the beginning of the paragraph is used for all Reynolds numbers. As $Re \to \infty$, the separation point's progression with time obtained analytically by the present third-order expansion is compared with that by Collins & Dennis (1973*a*, *b*) in table 3. The agreement is excellent, especially at small times, as expected. The trajectory of zero wall shear given in Sears & Telionis (1975), based on Telionis & Tsahalis (1974), also shows good agreement with the present results, except at the initiation of the zero wall shear. We did not encounter particular difficulty between $0{\cdot}6 < T < 0{\cdot}8$, as reported in Sears & Telionis (1975) in the calculation of radial velocity at $Re = \infty$. The comparison of the progression of the separation point at finite Reynolds numbers between Collins & Dennis (1973*b*) and the present result is made in table 4. As expected, the higher the Reynolds number, the better the agreement.

By manipulating the radial and tangential momentum equations, we can

θ	180	170	160	150	140	130	120	110
				$Re = 100, R_d = 200$				
Collins & Dennis (1973*b*, figure 6)	0·445	0·46	0·49	0·54	0·64	0·88	1·4	
Present	0·401	0·408	0·433	0·479	0·561	0·717	1·100	1·923
				$Re = 500, R_d = 1000$				
Collins & Dennis (1973*b*, figure 6)	0·371	0·39	0·40	0·45	0·51	0·64	0·93	1·6
Present	0·350	0·355	0·375	0·410	0·472	0·582	0·808	1·711

TABLE 4. Comparison of progression of separation point at finite Reynolds numbers

derive an expression for the pressure coefficient based on the pressure at the forward stagnation point,

$$C_p^0 = \frac{p(\theta)-p_0}{\frac{1}{2}\rho U_0^2} = \frac{2}{Re}\int_0^\theta \left(\frac{\partial\omega}{\partial r}\right)_{r_0} d\theta. \tag{45}$$

Using (44), we get

$$\begin{aligned} C_p^0 = &\left[-4+\left(\frac{303}{4}-84\sqrt{2}-\frac{68}{\pi^{\frac{1}{2}}}+138(2/\pi)^{\frac{1}{2}}-\frac{32}{3\pi\pi^{\frac{1}{2}}}+\frac{232}{5\pi}\right)\frac{T^{\frac{1}{2}}}{Re^{\frac{1}{2}}}\right.\\ &\left.-\left(28\sqrt{2}+\frac{232}{15\pi}-28\sqrt{2}\right)\frac{T}{Re}\right]\sin^2\theta\\ &+\left[-\left(18-\frac{30}{\pi^{\frac{1}{2}}}\right)Re^{-1}-\frac{4}{\pi^{\frac{1}{2}}}Re^{-\frac{1}{2}}T^{-\frac{1}{2}}+\frac{15}{\pi^{\frac{1}{2}}}\frac{T^{\frac{1}{2}}}{Re^{\frac{3}{2}}}\right.\\ &\left.+\left(\frac{64}{45\pi^2}+\frac{27\sqrt{3}-11}{30}-\frac{7}{12}\right)\frac{16}{3\pi^{\frac{1}{2}}}\frac{T^{\frac{3}{2}}}{Re^{\frac{1}{2}}}\right](1-\cos\theta)\\ &-\left(\frac{64}{27\pi^2}+\frac{27\sqrt{3}-20}{6}-\frac{3}{2}\right)\frac{16}{3\pi^{\frac{1}{2}}}\frac{T^{\frac{3}{2}}}{Re^{\frac{1}{2}}}(1-\cos^3\theta). \end{aligned} \tag{46}$$

The square-root time singularity in the second bracket of (46) is due, obviously, to the impulsive start.

The pressure coefficient C_p^0 is plotted in figures 9 and 10 for several Reynolds numbers. In order to perceive the tendency of the pressure distribution toward that at a later time, we plotted the curves up to a normalized time of 1·8. Although our expansion may not be valid at this time, it nevertheless indicates the basic behaviour of the pressure distribution. In the limiting case, $Re\to\infty$, the pressure coefficient is identical to that of the potential flow, as expected.

The drag on the cylinder has two parts, the form or pressure drag and the skin-friction drag. The pressure drag coefficient can be expressed as a vorticity quantity

$$C_{D_p} = \frac{D_p}{\rho U_0^2 r_0} = -\frac{2}{Re}\int_0^\pi \left(\frac{\partial\omega}{\partial r}\right)_{r_0}\sin\theta\, d\theta.$$

Using the vorticity gradient on the cylinder from (44), we get

$$\begin{aligned} C_{D_p} = &\,2\pi^{\frac{1}{2}}Re^{-\frac{1}{2}}T^{-\frac{1}{2}}+\pi\left(9-\frac{15}{\pi^{\frac{1}{2}}}\right)Re^{-1}-\frac{15}{2\pi^{\frac{1}{2}}}\frac{T^{\frac{1}{2}}}{Re^{\frac{3}{2}}}\\ &+2\pi^{\frac{1}{2}}\left[\left(\frac{108\sqrt{3}-89}{30\pi}+\frac{128}{135\pi^2}-\frac{11}{12}\right)+3\left(\frac{64}{45\pi^2}+\frac{27\sqrt{3}-11}{30\pi}-\frac{7}{12}\right)\right]\frac{T^{\frac{3}{2}}}{Re^{\frac{1}{2}}}. \end{aligned} \tag{47}$$

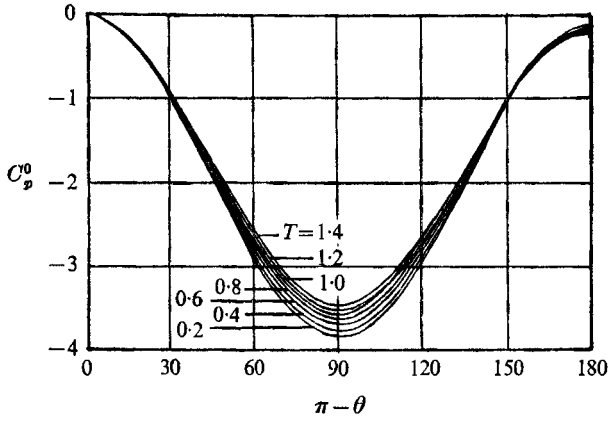

FIGURE 9. Pressure coefficient at $R_d = 2Re = 20000$.

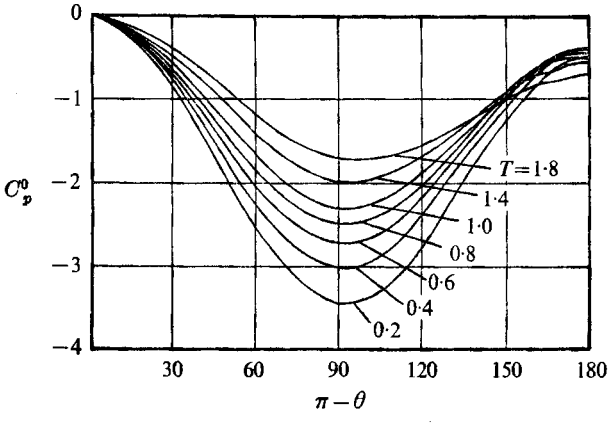

FIGURE 10. Pressure coefficient at $R_d = 2Re = 1000$.

The square-root singularity in time in (47) can be explained as the result of the impulsive nature of the cylinder motion. At the start of the motion, the cylinder displaces the fluid particles on the surface with infinite acceleration. The cylinder experiences, therefore, an infinite resistance of the fluid to its impulsive motion.

Expressing also the skin-fraction drag as a vorticity quantity, and using (43), we get

$$C_{D_f} = \frac{D_f}{\rho U_0^2 r_0} = \frac{2}{Re}\int_0^\pi (\omega)_{r_0} \sin\theta\, d\theta$$
$$= 2\pi^{\frac{1}{2}} T^{-\frac{1}{2}} Re^{-\frac{1}{2}} + \frac{\pi}{Re} + \frac{15}{2}\pi^{\frac{1}{2}}\frac{T^{\frac{1}{2}}}{Re\,Re^{\frac{1}{2}}}$$
$$- 2\pi^{\frac{1}{2}}\left[\left(\frac{108\sqrt{3}-89}{30\pi} + \frac{128}{135\pi^2} - \frac{11}{12}\right) + 3\left(\frac{64}{45\pi^2} + \frac{27\sqrt{3}-11}{30\pi} - \frac{7}{12}\right)\right]\frac{TT^{\frac{1}{2}}}{Re^{\frac{1}{2}}}. \quad (48)$$

At the start of the impulsive motion, a discontinuity in the tangential velocity exists on the surface. This discontinuity causes an infinite shear stress, and consequently gives rise to infinite drag, as indicated by the square-root singularity in (48). After the start, the vorticity diffuses, and the finite velocity jump

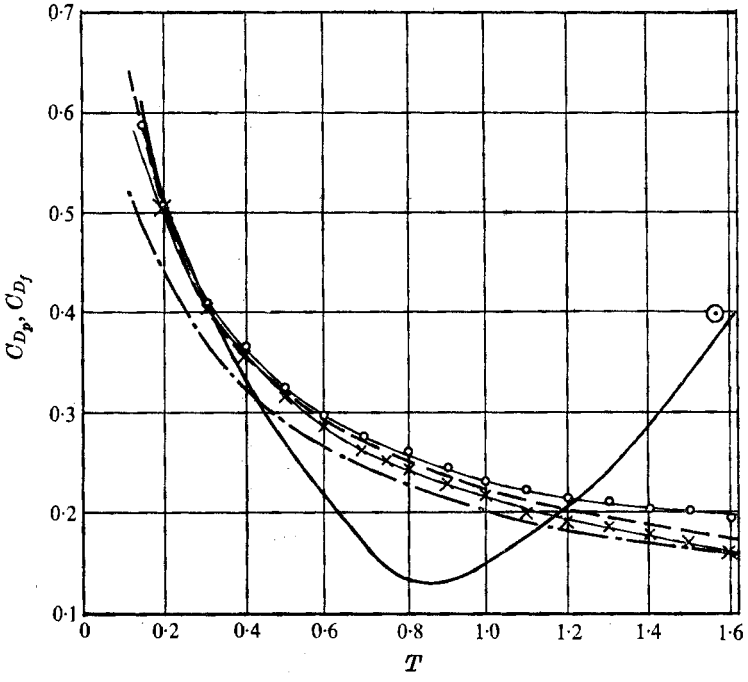

FIGURE 11. Pressure and skin-friction drag coefficients at $R_d = 2Re = 500$. ⊙, Schwabe (1943). Panikker & Lavan (1975): ———, C_{D_p}; — · —, C_{D_f}. – – – –, C_{D_p} and C_{D_f}, second order (Wang 1967); —○—○—, C_{D_p}, third order; – × – × –, C_{D_f}, third order.

near the surface is spread over a small but finite thickness. The magnitude of the shear stresses reduces, and skin-friction drag decreases. We observe that the leading terms in (48) and (47) are identical, so that at the start of the motion the contributions of the skin-friction drag and the pressure drag to the total drag are equal.

The time history of pressure drag (47) and of skin-friction drag (48) at $R_d = 2Re = 500$ are shown in figure 11, which is essentially Panikker & Lavan's (1975, figure 6). It is seen that the third-order expansion agrees better than the second-order with their numerical solution. Their pressure drag reaches a minimum at $T = 0{\cdot}9$, then rises because of the growth of separated flow region, and agrees with the first experimental point of Schwabe (1943). Since the present analytic solution is valid for $T < 1$, at $R_d = 500$ we could infer $T \leqslant 0{\cdot}5$. On account of (2) and (3), for higher Reynolds number, T may be closer to 1, or even a little beyond. The total drag coefficient is

$$C_D = \frac{D}{\rho U_0^2 r_0} = 4\pi^{\frac{1}{2}} Re^{-\frac{1}{2}} T^{-\frac{1}{2}} + \pi\left(9 - \frac{15}{\pi^{\frac{1}{2}}}\right) Re^{-1}, \tag{49}$$

adding (47) to (48). The time history of drag (49) at $R_d = 2Re = 500$ is plotted in figure 12, after Panikker & Lavan (1975, figure 7). It is seen that the present third-order solution is in excellent agreement with Collins & Dennis's (1973*a*), extended. For $T \leqslant 0{\cdot}05$, agreement between the present result and the numerical computation of Panikker & Lavan (1975) is good. The numerical value of Thoman

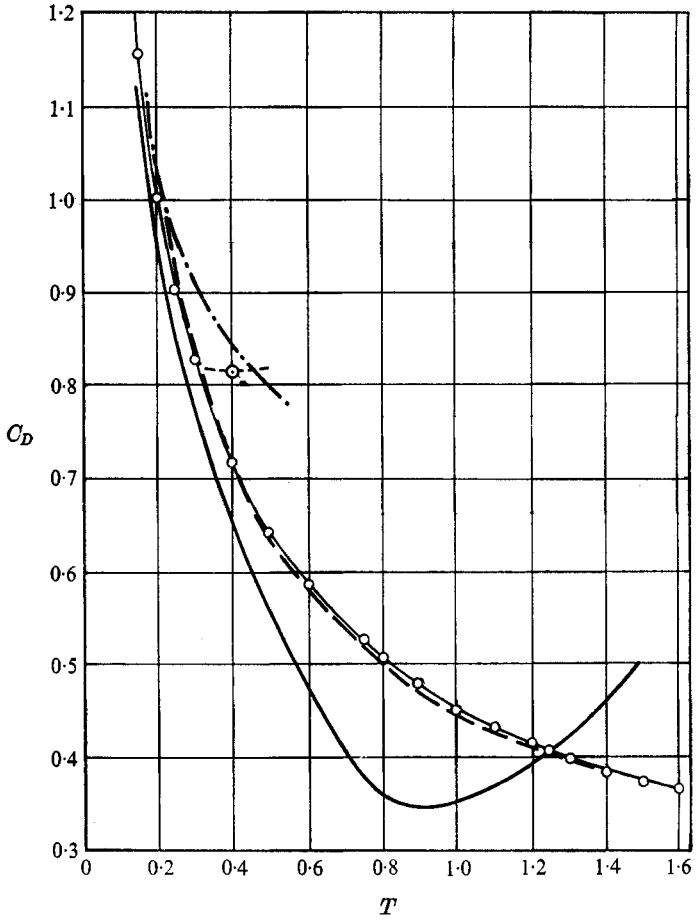

FIGURE 12. Drag coefficient at $R_d = 2Re = 500$. ⊙, Thoman & Szewczyk (1969), $R_d = 600$; ····, Collins & Dennis (1973*a*); ——, Panikker & Lavan (1975); —·—, second order Wang (1967); —○—○—, third order.

& Szewczyk (1969) is too high. The total drag rises at $T = 0{\cdot}9$ owing to the increase of pressure drag. This trend is also shown in other numerical computations, except those of Jain & Rao (1969, figure 4), where the drag coefficient decreases monotonically with time. The drag coefficient for various Reynolds numbers is plotted in figure 13. The drag coefficients in the limiting case $Re \to \infty$ are plotted in figure 14.

8. Padé approximation

The flow properties we developed are presented as a truncated double power series in time and Reynolds number. Our interest is in the time change of those properties at a constant Reynolds number. We therefore fix the Reynolds number in those expressions, and let the series proceed in powers of $T^{\frac{1}{2}}$. The maximum number of terms in the series is five. Since there are not enough terms to use the

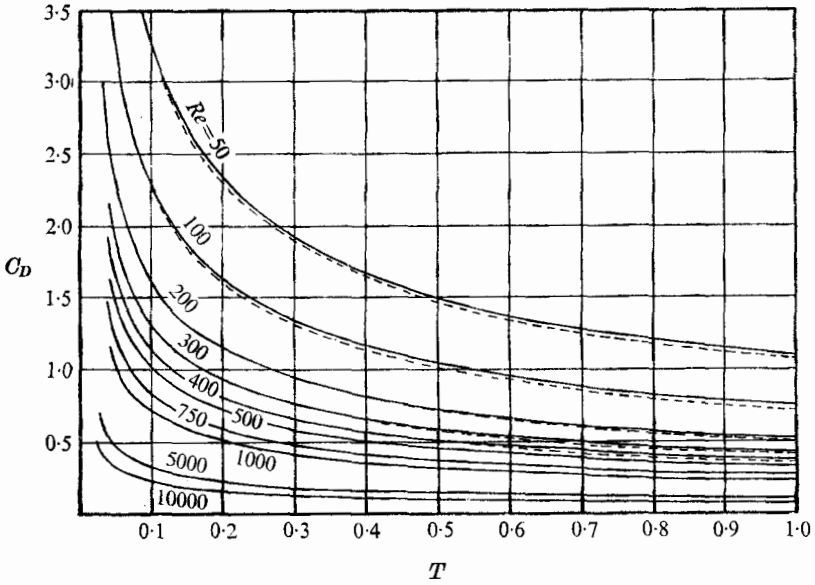

FIGURE 13. Drag coefficient at $R_d = 2Re$ = finite. – – –, Padé approximant [1/1].

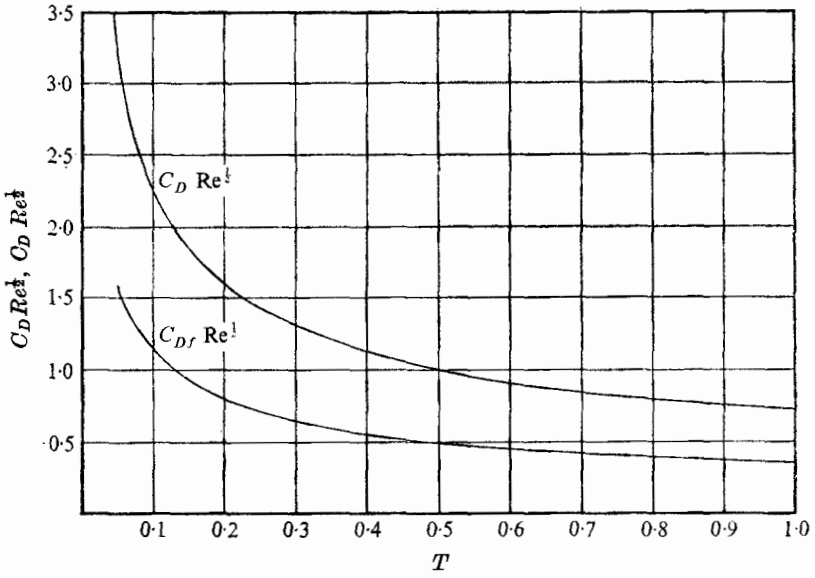

FIGURE 14. Drag coefficient at $R_d = 2Re = \infty$.

various techniques of series improvement (Van Dyke 1974), we are left with the Padé approximants (Baker 1975). The highest Padé diagonal we can use is [2/2], which requires knowledge of the first five coefficients.

The first two Padé diagonals for the power series

$$S(\epsilon) = \sum_{n=0} a_n \epsilon^n$$

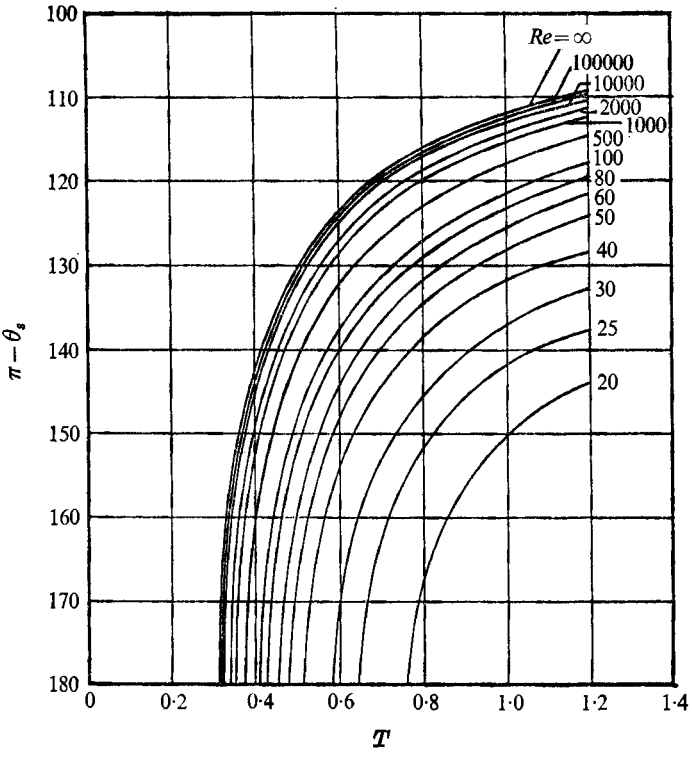

FIGURE 15. Progression of separation point: Padé approximant [2/2].

are

$$[1/1] = \frac{a_0 a_1 + (a_1^2 - a_0 a_2)\epsilon}{a_1 - a_2 \epsilon},$$

$$[2/2] = \frac{a_0(a_2^2 - a_1 a_3) + [a_1(a_2^2 - a_1 a_3) + a_0(a_1 a_4 - a_2 a_3)]\epsilon}{(a_2^2 - a_1 a_3) + (a_1 a_4 - a_2 a_3)\epsilon + (a_3^2 - a_2 a_4)\epsilon^2}$$
$$+ \frac{[a_0(a_3^2 - a_2 a_4) + a_1(a_1 a_4 - a_2 a_3) + a_2(a_2^2 - a_1 a_3)]\epsilon^2}{(a_2^2 - a_1 a_3) + (a_1 a_4 - a_2 a_3)\epsilon + (a_3^2 - a_2 a_4)\epsilon^2}.$$

The [2/2] Padé approximant was applied to (43) and equated to zero. This series governs the progression of the separation point on the cylinder. The progression of the separation point on the cylinder is plotted in figure 15. Comparing the results with figure 7, there is close agreement for Reynolds numbers higher than 500 or even 100. For Reynolds numbers below 500, the time for the initial separation at the rear stagnation point, as predicted by the Padé approximant, is later than that calculated by (43). The asymptotic steady-state separation angle is seen also to be somewhat closer to the rear stagnation point.

The initial time of separation at the rear stagnation point is plotted against Reynolds number in figure 8. The second- and third-order expansions are plotted in the same figure. The Padé approximant is very close to the third expansion. It does predict somewhat shorter times of initial separation for Reynolds numbers higher than 500, and longer separation times for Reynolds numbers below 500.

The Padé approximant [1/1] was applied to the drag coefficient. The results are plotted in figure 11. The drag coefficient calculated by Padé approximants is somewhat lower.

9. Conclusion

The initial flow over an impulsively started circular cylinder was solved by using the method of matched asymptotic expansions to the third order. The solution should be valid for $T \equiv U_0 t^*/r_0 < 1$, $Re \equiv U_0 r_0/\nu_0 > 100$. Because of (2) and (3), the solution may be stretched to $T \approx 1$ for higher Reynolds numbers.

The two basic characteristics of the flow (the vorticity and the vorticity strength on the surface) were first derived, plotted and studied. At a finite time after the impulsive start, separation of the boundary layer starts at the rear stagnation point and progresses along the cylinder asymptotically to a final separation angle. The lower the Reynolds number, the longer the flow takes to start separating, and the closer to the rear stagnation point the final separation angle. Although the solution is not valid for small Reynolds numbers, figure 8 seems to indicate the existence of a limiting Reynolds number, below which separation will not take place.

Using the vorticity derivatives, the skin-friction drag, pressure drag, and pressure distribution on the cylinder were derived. All these quantities agree well with the computations of Collins & Dennis (1973*a*, *b*). (See e.g. figures 8, 11, 12; tables 1–4.) The skin-friction drag and pressure drag have the same magnitude at the start of the flow, which agrees with Collins & Dennis. The drag coefficient is compared with the recent numerical computation of Panikker & Lavan (1975). At $R_d = 2$, $Re = 500$, for $T \leqslant 0{\cdot}5$, the agreement is good.

The singular behaviour of flow properties at very small times could be treated from the viewpoint of kinetic theory as in Rayleigh's problem. (See e.g. Yang & Lees 1956.) For large times, the present problem could be treated as indicated in Robins & Howarth (1972), after Proudman & Johnson (1962). For intermediate times, one may have to resort to direct numerical computation.

Padé approximants were used in an attempt to improve the results. The Padé approximants agreed very well with the third-order expansion, indicating that, probably, only minor improvements can be gained by calculating higher-order approximations.

The authors wish to thank Professor H. K. Cheng for bringing to their attention the question of unsteady boundary-layer separation points and the technique of Padé approximants. The senior author thanks Professor H. K. Cheng and Professor K. Stewartson for helpful discussions.

REFERENCES

BAKER, G. A. 1975 *Essentials of Padé Approximant.* Academic.

BELCHER, R. J., BURGGRAF, O. R., COOKE, J. C., ROBINS, A. J. & STEWARTSON, K. 1972 *Recent Research on Unsteady Boundary Layers*, vol. 2 (ed. E. A. Eichelbrenner). Quebec: Laval University Press.

COLLINS, W. M. & DENNIS, S. C. R. 1973*a* *Quart. J. Mech. Appl. Math.* **26**, 53.

COLLINS, W. M. & DENNIS, S. C. R. 1973*b* *J. Fluid Mech.* **60**, 105.

JAIN, P. C. & RAO, K. S. 1969 *Phys. Fluids Suppl.* **12**, II–57.

PANIKKER, P. K. K. & LAVAN, Z. 1975 *J. Comp. Phys.* **18**, 46.

PROUDMAN, I. & JOHNSON, K. 1962 *J. Fluid Mech.* **12**, 161.

RILEY, N. 1975 *SIAM Rev.* **17**, 278.

ROBINS, A. J. & HOWARTH, J. A. 1972 *J. Fluid Mech.* **56**, 161.

ROSENHEAD, L. (ed.) 1963 *Laminar Boundary Layer.* Oxford: Clarendon Press.

SCHLICHTING, H. 1968 *Boundary Layer Theory.* McGraw-Hill.

SCHWABE, M. 1943 *N.A.C.A. Tech. Memo.* no. 1039.

SEARS, W. R. & TELIONIS, D. P. 1975 *SIAM J. Appl. Math.* **28**, 215.

TELIONIS, D. P. & TSAHALIS, D. T. 1974 *Acta Astronautica*, **1**, 1487.

THOMAN, D. C. & SZEWCZYK, A. A. 1969 *Phys. Fluids Suppl.* **12**, II–76.

VAN DYKE, M. 1974 *Quart. J. Mech. Appl. Math.* **27**, 423.

VAN DYKE, M. 1975 *Perturbation Methods in Fluid Mechanics.* Parabolic.

WANG, C. Y. 1967 *J. Math. Phys.* **46**, 195.

YANG, H. T. & LEES, L. 1956 *J. Math. Phys.* **24**, 195.